Direct Observation of Strong Ion Coupling in Laser-Driven Shock-Compressed Targets

A. Ravasio,[1] G. Gregori,[2] A. Benuzzi-Mounaix,[1] J. Daligault,[3] A. Delserieys,[4] A. Ya. Faenov,[5] B. Loupias,[1] N. Ozaki,[1] M. Rabec le Gloahec,[1] T. A. Pikuz,[5] D. Riley,[4] and M. Koenig[1]

[1]*Laboratoire pour l'Utilisation de Lasers Intenses, UMR7605, CNRS–CEA, Université Paris VI–Ecole Polytechnique, 91128 Palaiseau Cedex, France*

[2]*CCLRC, Rutherford Appleton Laboratory, Chilton, Didcot OX11 0QX, United Kingdom, Clarendon Laboratory, University of Oxford, Parks Road, Oxford, OX1 3PU, United Kingdom*

[3]*Theoretical Division, Los Alamos National Laboratory, Los Alamos, New Mexico 87545, USA*

[4]*School of Mathematics and Physics, Queens University of Belfast, Belfast BT7 INN, United Kingdom*

[5]*Multicharged Ions Spectra Data Center of VNIIFTRI, Russian Committee of Standards, Moscow Region, 141570, Russia*

(Received 7 June 2007; published 28 September 2007)

In this Letter we report on a near collective x-ray scattering experiment on shock-compressed targets. A highly coupled Al plasma was generated and probed by spectrally resolving an x-ray source forward scattered by the sample. A significant reduction in the intensity of the elastic scatter was observed, which we attribute to the formation of an incipient long-range order. This speculation is confirmed by x-ray scattering calculations accounting for both electron degeneracy and strong coupling effects. Measurements from rear side visible diagnostics are consistent with the plasma parameters inferred from x-ray scattering data. These results give the experimental evidence of the strongly coupled ionic dynamics in dense plasmas.

DOI: 10.1103/PhysRevLett.99.135006 PACS numbers: 52.50.Jm, 52.25.Os, 52.35.Fp

The study of extreme states of matter is of fundamental interest for the understanding of laboratory astrophysics [1], geophysics [2], and inertial confinement fusion experiments [3]. Of particular relevance is the so-called warm dense matter regime (WDM) characterized by near or above solid densities and by temperatures $\lesssim$100 eV. In this regime, matter consists of a plasma where ions are in a liquidlike, correlated state and electrons are degenerate. Correlations among the ions arise because their interaction energy overcomes their thermal energy, which is conveniently quantified by the dimensionless ion coupling parameter $\Gamma = [(ze)^2/(4\pi\epsilon_0 a k_B T_i)]$ where $a = (4\pi N_i/3)^{-1/3}$ is the Wigner-Seitz radius, Ni is the ionic particle density, and Ti is the temperature. In WDM, Γ is greater than unity, which provides a tremendous challenge to the theory [4]. The experimental approach is therefore essential.

Recently, x-ray scattering has been proven to be a successful technique in characterizing the macroscopic properties of WDM [5,6]. When the scattering wavelength $\lambda_s = 1/k = [\lambda_0/(4\pi \sin\theta/2)]$ (λ_0 is the probe x-ray wavelength and θ the scattering angle) becomes comparable to the plasma screening length (d), the spectrum of the scattered light directly reflects the collective response and dynamics of the plasma [7]. In this Letter we present the first experimental results on near collective x-ray scattering measurements (with $\lambda_s \sim d$) done on strongly coupled plasmas produced from shocked compressed aluminum targets.

The experiment was performed on the LULI 2000 laser facility at the Laboratoire pour l'Utilisation des Lasers Intenses (LULI), Ecole Polytechnique (France). We created a dense and compressed Al plasma by launching a shock wave into a solid 4.5 μm plastic (CH)/ 6 μm Al/ 4.5 μm CH multilayer foil, using one of the two 400 J frequency-doubled Nd-glass LULI2000 laser beams with a 1 ns square pulse. The plastic layers were necessary to both act as an ablator pusher on the front (laser) side and to prevent hydrodynamic expansion of the Al rear side. To eliminate large scale spatial modulations of intensity and to obtain a flat intensity profile in the focal spot [8], a phase zone plate (PZP) [9] was inserted in the beam. This resulted in a $\gtrsim$1 mm diameter focal spot having a 850 μm flat profile, giving an intensity $I_L \lesssim 10^{13}$ W/cm^2 on target. The second beam was focused on a titanium backlighter foil to generate an intense x-ray source (Ti He-α radiation and associated dielectronic satellite lines) in the range of 4.70–4.75 keV. Figure 1 shows a scheme of the experimental setup. The x-ray radiation scattered from the plasma was collected and spectrally resolved with a LiF (200) curved crystal coupled to a CCD (charge coupled

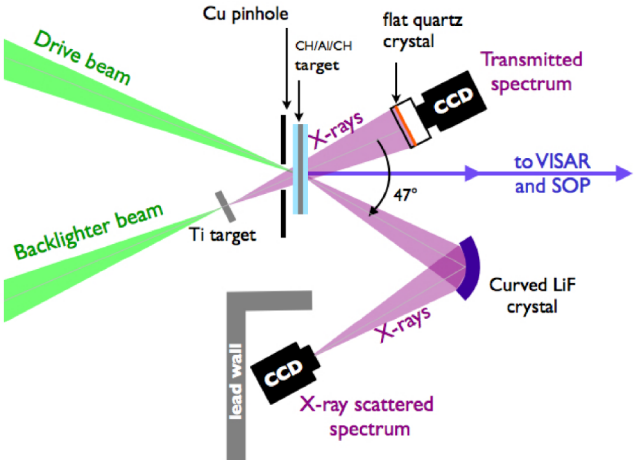

FIG. 1 (color online). Scheme of the experimental setup.

 © 2007 The American Physical Society

device) detector. The collection angle was 47°, small enough to probe the near collective scattering regime ($\alpha = 1/kd \approx 0.9$). A 1 mm pinhole on a Cu substrate was used to restrict x-ray illumination to the shocked part of the target. Test shots were taken and confirmed that no signal was observed when the sample was not in place. A second Si (111) flat crystal spectrometer, also coupled to a CCD, was set up to collect the transmitted Ti x rays from the source. This allowed us to monitor the spectral intensity of the source radiation at each shot. Two rear side optical diagnostics VISAR (velocity interferometer system for any reflector) and a temporally resolved self-emission were implemented in order to independently measure the plasma parameters and to cross check the scattering results. Under our experimental conditions, the equation of states of both Al [10] and CH [11] are presumably known with good accuracy, so that the shock velocity measurement only is sufficient to deduce all the other plasma parameters (electron temperature, density, and pressure). The instantaneous shock velocity in the rear plastic layer was obtained using VISAR interferometers coupled to a streak camera [12]. Figure 2(a) shows a recorded VISAR image generated by the reflection of a low intensity laser probe beam incident on the target rear side. Since the shock is strong enough, the CH goes through an insulator-to-metallic phase transition and it reflects the probe light. Therefore, the measurement of the associated fringe shift in the interference pattern gives the instantaneous shock velocity, as presented in Fig. 2(b). The shock propagates at 13 km/s when it goes into the plastic and it decays down to ~10 km/s before breaking out into vacuum. We have also compared the shock velocity results in the rear plastic layer with a time resolved self-emission diagnostic [11,13]. The increase of temperature associated to the compression causes the shocked plastic to emit thermal radiation which is transmitted through the transparent, unshocked CH. A mean shock velocity of 12.2 ± 0.6 km/s was obtained, in good agreement with VISAR measurements. We then have used 1D hydrodynamic simulations (MULTI [14]) to infer the time evolution of the Al plasma parameters, since we probed different plasma conditions (500 ps and 5 ns after the shock driver laser beam has reached its maximum intensity). The input parameters for the simulations were fixed in such a way to match the experimental shock speed in CH and thus giving a robust confidence on the Al state at late times. Results of the hydrodynamic simulations are shown in Fig. 3 for the electron density $N_e = Z^* N_i$, the electron temperature T_e, and the ionization Z^*, averaged over the probing duration ($\gtrsim$1 ns). Moreover, the predicted temperature in the CH is in good agreement with the experimental results ($T_e \sim 0.8$ eV) given by the self-

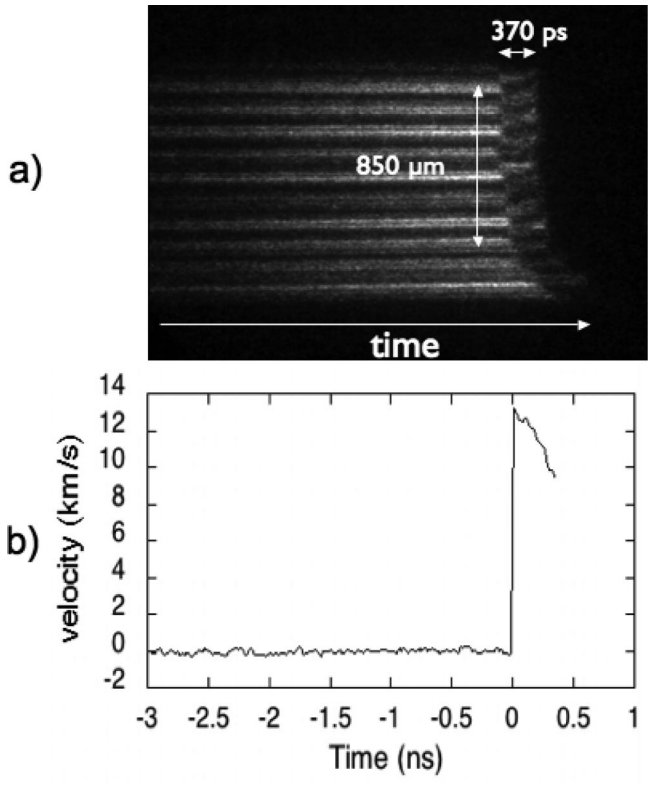

FIG. 2. (a) Experimental image from the VISAR diagnostic. The shock is planar over ~850 μm, consistently with the PZP focal spot. The shock transit time in the last CH layer is ~375 ps (b) Corresponding deduced shock velocity in the rear CH layer.

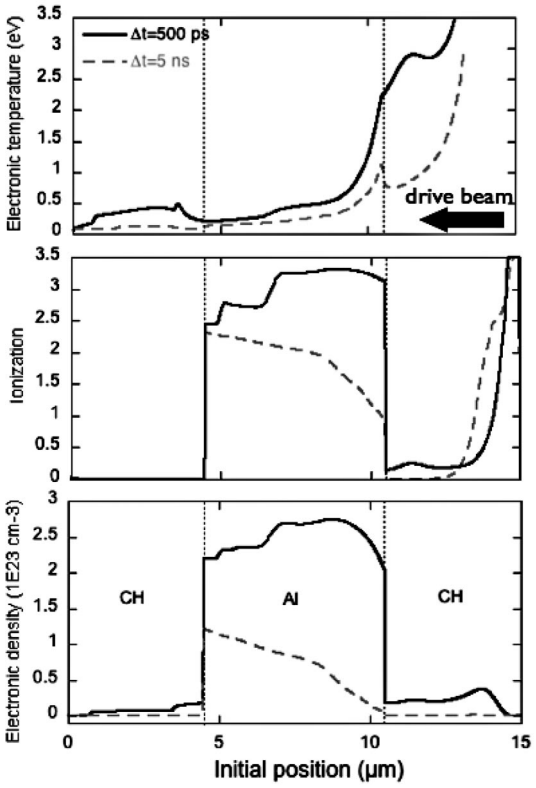

FIG. 3. Electron density (a), ionization (b), and temperature (c) from hydrodynamic simulations at 500 ps (solid black line) and 5 ns (dotted gray line) after the maximum laser intensity. The same simulations reproduce the measured shock velocity in the last CH layer.

emission diagnostics, which acts as a pyrometer [11]. At early times (500 ps after the laser peak intensity and during 1 ns), the Al layer is completely shocked and the resulting plasma is considerably dense and cold. In the Al layer $N_e \sim 2.5 \times 10^{23}$ cm^{-3} while $T_e \sim 0.35$ eV and $Z* \sim 2.9$. At these densities energy relaxation times are much shorter than the characteristic hydrodynamic time scale and local thermodynamic equilibrium is reached with $T_i = T_e$. The electrons exhibit degeneracy ($T_e/T_F \sim 0.03$, with T_F being the Fermi energy) and a low level of coupling. On the contrary, the ions are highly coupled, with a coupling parameter $\Gamma \sim 240$. In multicomponent plasmas the effect of screening tends to attenuate the electrostatic interactions and it has been suggested [4] that a more appropriate coupling parameter is $\Gamma_s = \Gamma \exp(-k_s a) \sim 19$, where $1/k_s$ is the short-range screening length and a the Wigner-Seitz radius. Since both Γ and Γ_s are large, it is reasonable to expect that ion-ion coupling plays an important role in our experimental conditions. In Ref. [15] the microscopic dynamics of the case of one component plasma (OCP) in strongly coupled regimes was investigated. It was shown that for $\Gamma \gg 50$ the OCP shows an increasingly correlated fluidlike behavior undergoing to Wigner crystallization at $\Gamma \gtrsim 175$ [4,15]. We speculate that for our conditions, even if crystallization has not occurred, the highly correlated ions drive the formation of incipient long-range order, which is preserved during the x-ray scattering time [16]. In this picture, the ion motion can be described as a sum of two different terms: an oscillation (vibration) around the instantaneous center of mass and a global translation (diffusion) of the center of mass. The two mechanisms contribute to the total elastic cross section $\sigma_{\mathrm{II}}^{\mathrm{el}}(k)$, in the zero phonon approximation given by [17–19]

$$\sigma_{\mathrm{II}}^{\mathrm{el}}(k) = S_{ii}(k)(1 - e^{-2W}), \tag{1}$$

where Bragg scattering has been neglected for angles which do not satisfy the Bragg condition, as in the case for this experiment. In Eq. (1) the first term, $S_{ii}(k)$, corresponds to the ion-ion density correlation function [4]. In the case of a strongly coupled plasma in the collective regime (i.e., for k small), it is a weak function of the plasma temperature (see, e.g., Ref. [19]). The second term of Eq. (1), $(1 - e^{-2W})$, corresponds to the Debye-Waller thermal smearing due to the ion vibrations [16], W being the Debye-Waller factor defined in Eq. (50) of Ref. [19]. Its appearance does not require a strict crystalline lattice, but it naturally arises as a consequence of the ion fluctuations. In the long wavelength limit ($k \to 0$), at sufficiently low $T_e (= T_i)$, $W \propto 1/\Gamma$ [19,20]. Thus, $\sigma_{\mathrm{II}}^{\mathrm{el}} \propto 1/\Gamma$ at large coupling parameters. This implies that the formation of long-range order must be followed by a significant reduction of the elastic scatter term in the measured spectrum. This effect is evidenced in our experimental data, as shown in Fig. 4. Figure 4(b) shows the scattered spectrum from the shocked plasma when the delay between the backlighter

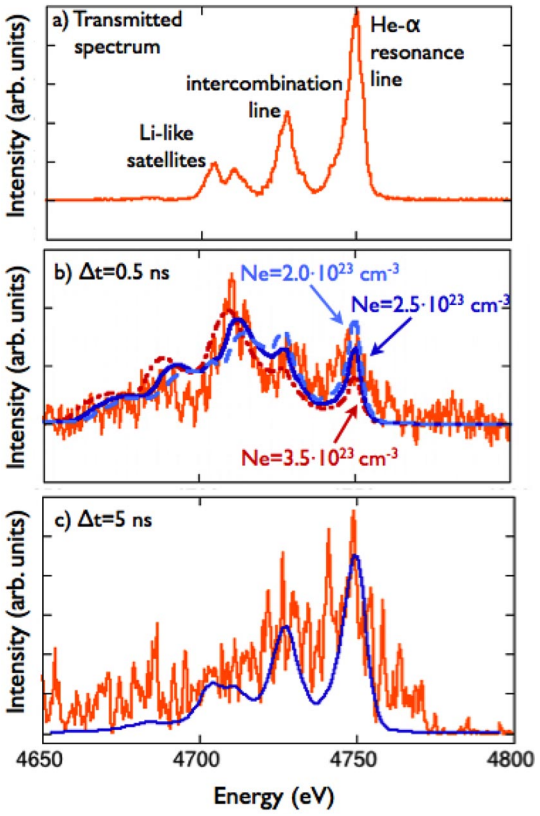

FIG. 4 (color online). Ti source spectrum as recorded by the spectrometer looking at the transmitted light (a) and scattered data at 500 ps (b) and 5 ns (c) after the intensity peak of the shock drive pulse.

and the driver beam was 500 ps. The transmitted spectrum of the Ti source through the sample, for the same shot, is given in Fig. 4(a). We notice that in the transmitted spectrum the intensity of the Li-like satellites is lower than the He-α lines, as typically measured in Ti foils irradiated at comparable intensities [21]. In the scattered spectrum, the high frequency fluctuations are associated to the low signal-to-noise ratio, due to the extremely weak value of the Thomson scattering cross section. It is now evident that, differently from the transmitted signal, the predominant feature lies at the satellites position. There, the scattering signal is the sum of both the elastically scattered photons from the Li-like satellites and the inelastically scattered x-rays from free and weakly bound electrons [22], which are downshifted in energy. The inelastic component, thus, appears stronger than the elastic one, in contrast with results obtained in weakly coupled plasmas [23], where coupled ions oscillations do not play a major role. In that case $\sigma_{\mathrm{II}}^{\mathrm{el}}/\sigma^{\mathrm{inel}} \sim Z_b^2/Z^*$ [22], where σ^{inel} is the inelastic cross section and Z_b the number of bound electrons per ion. In our case, due to the W dependence, $\sigma_{\mathrm{II}}^{\mathrm{el}}/\sigma^{\mathrm{inel}} \sim Z_b^2/Z^*$, which significantly enhances the inelastic contribution. This is confirmed by calculations of the scattered signal, evaluated with a model that fully accounts for electron degeneracy, strong coupling effects,

and self-energy corrections to the ion mass [18,19,24], necessary for finite T_e and k. Our experimental data are indeed well reproduced including the Debye-Waller term in the elastic cross section. The total scattering cross section also includes the inelastic scatter from free and bound electrons as described in Refs. [22,7]. In the simulation we have convolved the calculated scattering cross section with the Ti spectrum given in Fig. 4(a). The results are shown in Fig. 4(b), superimposed to the data. To account for both the time evolution and spatial gradients during the probing time, individual scattering spectra at different positions in space and time have been added together. The best match [solid blue (or dark gray) line in Fig. 4] with the experimental data is obtained for values of the electronic density, temperature, and ionization state in optimal agreement with those deduced from hydrodynamic simulations (Fig. 3). The low intensity of the elastic component is well reproduced as well as the more intense inelastic feature, shifted at the satellites energy position.

In Fig. 4(b) we also show two other calculated spectra obtained with the electronic density, set to 3.5×10^{23} cm^{-3} [dotted red (or gray) line] and 2×10^{23} cm^{-3} [dashed light blue (or light gray) line]. We can notice that the intensity of the elastic component is sensitive to electronic density and it decreases when the electron density increases, in agreement with the $1/\Gamma$ scaling. Moreover, the inelastic scattered component is downshifted in energy by $\approx\sqrt{(\hbar^2k^2/2m)^2 + \hbar^2\omega_p^2}$ (m is the electron mass and ω_p the plasma frequency) and thus also changes with the electron density. We have also tested the sensitivity with the electronic temperature (=ionic temperature). A similar effect on the elastic scattering intensity is found, where now a stronger damping is obtained for higher T_e. Indeed, at a fixed electronic density, set to have the correct spectral shift, the ion-ion correlations become stronger for a lower temperature and the correction associated to the Debye-Waller factor more important. Sensitivity analysis shows that the error in the temperature measurement is ± 0.2 eV.

In order to probe a significantly different plasma state, we have changed the delay between the main drive laser beam and the x-ray source up to 5 ns. At this time the shock has broken out from the target rear surface and a rarefaction wave travels back into the target. The predicted state is also shown in Fig. 3, where we deduce a $N_e = 8.5 \times 10^{22}$ cm^{-3}, a $T_e \sim 0.25$ eV, and $Z^* \sim 2.1$. Under these conditions the ion coupling parameter is lower ($\Gamma_s \sim 5$) and the effects due to ion correlations are softened [15]. The results are shown in Fig. 4(c), where we can notice that the experimental scattered spectrum does evidence this behavior, the elastic component being now the dominant feature. This is due to a weaker correction from the Debye-Waller factor, consistent with earlier results obtained in the noncollective regime [23]. The x-ray spectrum calculated using the plasma parameters from the hydrodynamic simulation again fits the data.

Accounting for changes in laser energy between shots we find that the integrated signals in Figs. 4(b) and 4(c) are approximately the same. On the other hand, the high frequency noise prevents direct comparison of the absolute signal levels, leaving it to a future experiment. In conclusion, we have reported the measurement of quasicollective x-ray Thomson scattering from shock-compressed targets. We have evidenced the effects of ion correlations on the scattered spectra, which suppress the elastic component outside the Bragg peaks. Moreover, the x-ray scattering technique was cross checked with optical diagnostics currently used in shock wave experiments, showing good agreement and underlying the great potential of this diagnostic in the investigation of dense and highly coupled plasmas. This technique can be implemented in future studies of nonequilibrium phase transitions and ultrafast structural processes in WDM, in analogy with successful work already established in the solid state community [25].

This work was supported by the Access to Research Infrastructures activity (E.U. Contract No. RII3-CT-2003-506350, Laserlab Europe). The authors would like to thank Dr. S. H. Glenzer and Dr. G. Faussurier for useful discussions.

[1] B. A. Remington *et al.*, Science **284**, 1488 (1999); Rev. Mod. Phys. **78**, 755 (2006).
[2] G. Huser *et al.*, Phys. Plasmas **12**, 060701 (2005).
[3] J. Nuckolls *et al.*, Nature (London) **239**, 139 (1972).
[4] S. Ichimaru, *Statistical Plasma Physics* (Addison-Wesley, Reading, MA, 1991).
[5] D. Riley *et al.*, Phys. Rev. Lett. **84**, 1704 (2000).
[6] G. Glenzer *et al.*, Phys. Rev. Lett. **98**, 065002 (2007).
[7] G. Gregori *et al.*, Phys. Rev. E **67**, 026412 (2003).
[8] M. Koenig *et al.*, Phys. Rev. E **50**, R3314 (1994).
[9] T. H. Bett *et al.*, Appl. Opt. **34**, 4025 (1995).
[10] K. S. Holian, LANL Report No. LA-10160-MS UC-34, 1984.
[11] M. Koenig *et al.*, Phys. Plasmas **12**, 012706 (2005).
[12] L. M. Barker and R. E. Hollenbach, J. Appl. Phys. **43**, 4669 (1972); P. M. Celliers *et al.*, Rev. Sci. Instrum. **75**, 4916 (2004).
[13] R. L. Kauffman *et al.*, Rev. Sci. Instrum. **66**, 678 (1995).
[14] R. Ramis *et al.*, Comput. Phys. Commun. **49**, 475 (1988).
[15] J. Daligault, Phys. Rev. Lett. **96**, 065003 (2006).
[16] D. A. Baiko *et al.*, Phys. Rev. Lett. **81**, 5556 (1998).
[17] B. E. Warren, *X-Ray Diffraction* (Dover, New York, 1976).
[18] G. Gregori *et al.*, Phys. Rev. E **74**, 026402 (2006).
[19] G. Gregori *et al.*, High Energy Density Phys. **3**, 99 (2007).
[20] E. L. Pollock and J.-P. Hansen, Phys. Rev. A **8**, 3110 (1973).
[21] D. Riley *et al.*, Plasma Sources Sci. Technol. **11**, 484 (2002).
[22] G. Gregori *et al.*, Phys. Plasmas **11**, 2754 (2004).
[23] G. Glenzer *et al.*, Phys. Rev. Lett. **90**, 175002 (2003).
[24] W. D. Kraeft *et al.*, *Quantum Statistics of Charged Particles Systems* (Akademie-Verlag, Berlin, 1986).
[25] A. M. Lindenberg *et al.*, Science **308**, 392 (2005).